analytical chemistry

Letter

pubs.acs.org/ac

Multishell Au/Ag/SiO_2 Nanorods with Tunable Optical Properties as Single Particle Orientation and Rotational Tracking Probes

Kuangcai Chen,[†] Chia-Cheng Lin,[†] Javier Vela,* and Ning Fang*

Ames Laboratory, U.S. Department of Energy, and Department of Chemistry, Iowa State University, Ames, Iowa 50011, United States

Supporting Information

ABSTRACT: Three-layer core−shell plasmonic nanorods (Au/Ag/SiO_2−NRs), consisting of a gold nanorod core, a thin silver shell, and a thin silica layer, were synthesized and used as optical imaging probes under a differential interference contrast microscope for single particle orientation and rotational tracking. The localized surface plasmon resonance modes were enhanced upon the addition of the silver shell, and the anisotropic optical properties of gold nanorods were maintained. The silica coating enables surface functionalization with silane coupling agents and provides enhanced stability and biocompatibility. Taking advantage of the longitudinal LSPR enhancement, the orientation and rotational information of the hybrid nanorods on synthetic lipid bilayers and on live cell membranes were obtained with millisecond temporal resolution using a scientific complementary metal-oxide-semiconductor camera. The results demonstrate that the as-synthesized hybrid nanorods are promising imaging probes with improved sensitivity and good biocompatibility for single plasmonic particle tracking experiments in biological systems.

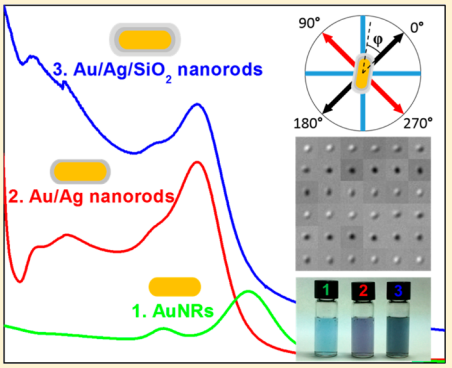

Single particle tracking (SPT) is a powerful tool to study the dynamics of cellular and molecular processes, such as membrane dynamics,[1,2] viral infection,[3] and intracellular transport.[4,5] A large collection of imaging probes, including fluorescent molecules,[6,7] quantum dots,[8,9] and plasmonic nanoparticles,[5,10−16] have been visualized with the aid of various optical microscopy techniques. While it has become a routine practice in SPT experiments to identify the trajectory of an imaging probe, it is more difficult to resolve the dipole orientation of the probe in real time, which may be essential in understanding the underlying biological functions. Recently, considerable efforts have been made to overcome this challenge. Techniques such as fluorescence polarization microscopy,[6−8] dark field polarization scattering,[10] defocused orientation and position imaging,[9,13] photothermal imaging,[11] correlation spectroscopy,[12,14] total internal reflection scattering microscopy,[15,17] and differential interference contrast (DIC) microscopy[18,19] have been developed for *single particle orientation and rotational tracking*, which was coined as SPORT.[19,20]

Gold nanorods (AuNRs) have been used extensively in SPORT experiments because of their high photostability, good biocompatibility, and most importantly, anisotropic optical properties arising from their localized surface plasmon resonance (LSPR). Great success has been achieved on the AuNR synthesis using seed-mediated methods to fabricate a variety of AuNRs with different sizes and aspect ratios and thus the resulting tunable extinction spectra across a wide spectral range.[21,22] Compared with gold nanocrystals of similar size, silver nanocrystals exhibit stronger LSPR responses with more intense electric field enhancement and stronger absorption and scattering. However, the synthesis of anisotropic silver nanorods (AgNRs), especially for the smaller sizes (<100 nm in length) that are better suited for biological studies, is more difficult than that of AuNRs in terms of size and shape uniformity control.[23,24] Since silver shares the same face centered cubic crystal structure with gold and their lattice mismatch is as small as 0.27%, AuNRs are suitable templates for epitaxial silver growth to form Au/Ag core−shell nanorods (Au/AgNRs).[25−30] The optical properties of Au/AgNRs can be finely tuned by controlling the aspect ratio of the AuNR cores and the amount of silver grown on the gold surface.[29] Moreover, the formation of Au/AgNRs induces multiple plasmonic bands that differ from single-component nanocrystals.

In view of the intrinsic cytotoxicity and unstable nature of the silver shells in aqueous solution,[23,31,32] encapsulation of Au/AgNRs within a thin silica layer to form a three-layer core−shell nanorod structure, which will be referred to as Au/Ag/SiO_2−NR in this Letter, can provide the necessary protection in biological imaging applications. The silica coating also improves the colloidal stability of Au/AgNRs, maintains the rod shape, and enables further surface functionalization with silane coupling agents for potential bioconjugation.[33−35] Surface modification of the silica shell usually involves covalent attachment; therefore, this avoids cysteine residue replacement

Received: February 12, 2015
Accepted: April 7, 2015
Published: April 7, 2015

DOI: 10.1021/acs.analchem.5b00604
Anal. Chem. 2015, 87, 4096−4099

of thiol ligands, which is often used in gold or silver surface functionalization.[36]

In the present study, Au/Ag/SiO_2−NRs were synthesized and tested for SPORT experiments. Millisecond/submillisecond temporal resolution was achieved in imaging the fast dynamics of Au/Ag/SiO_2−NRs rotating on synthetic lipid membranes and live cell membranes. To the best of our knowledge, this study demonstrates for the first time the development and application of hybrid core−shell nanorods as a new type of rotational probe.

The first step in synthesizing Au/Ag/SiO_2−NRs was to prepare AuNRs using a seed-mediated growth method in aqueous solution utilizing cetyltrimethylammonium bromide (CTAB) as capping agent to maintain colloidal stability.[21] The average diameter, length, and aspect ratio of the synthesized AuNRs obtained from the TEM images (Figure S1 in the Supporting Information) were 22.8 ± 3.2 nm, 52.6 ± 7.2 nm, and 2.3 ± 0.2, respectively. Their transverse and longitudinal LSPR wavelengths were centered at 517 and 632 nm, as shown in the UV−vis extinction spectrum (Figure 1, green curve).

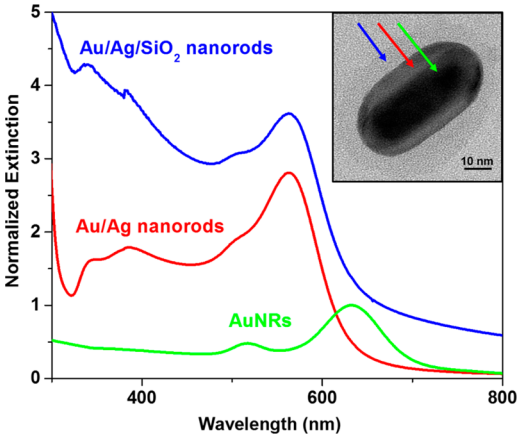

Figure 1. Normalized UV−vis extinction spectra of AuNRs, Au/AgNRs, and Au/Ag/SiO_2−NRs in water. All the spectra are normalized to the longitudinal dipolar plasmonic peak at 632 nm. The inset is a representative TEM image of Au/Ag/SiO_2−NR and the colored arrows indicate gold-only (green), silver-coated (red), and silica-coated (blue) samples.

In the second step of synthesis, a thin silver layer (~7 nm thick) was deposited onto the AuNRs following a published procedure.[25,37] The thickness of the silver coating was controlled by adjusting the amount of $AgNO_3$ precursor. Upon the addition of silver onto the AuNR cores, the extinction peak at the lowest energy wavelength was blue-shifted and new plasmonic bands appeared at higher energies. Figure S2 in the Supporting Information illustrates the UV−vis extinction spectra of the Au/AgNRs with three Ag/Au molar ratios of 0.11, 0.22, and 0.34. As the Ag/Au molar ratio increases, the silver shell becomes thicker and the longitudinal LSPR wavelength is blue-shifted from 632 nm to 575, 537, and 503 nm, respectively. This blue shift is attributed to the reduced aspect ratio of the nanorods after the silver coating and the increased silver loading on gold dominates the optical properties. This plasmonic band shift can be used to estimate the Ag shell thickness as well as to direct further syntheses.[26,28,30] The Au/AgNRs with the Ag/Au molar ratio of 0.11 maintained the original cylindrical rod shape. Figure S2 curve b in the Supporting Information shows the four

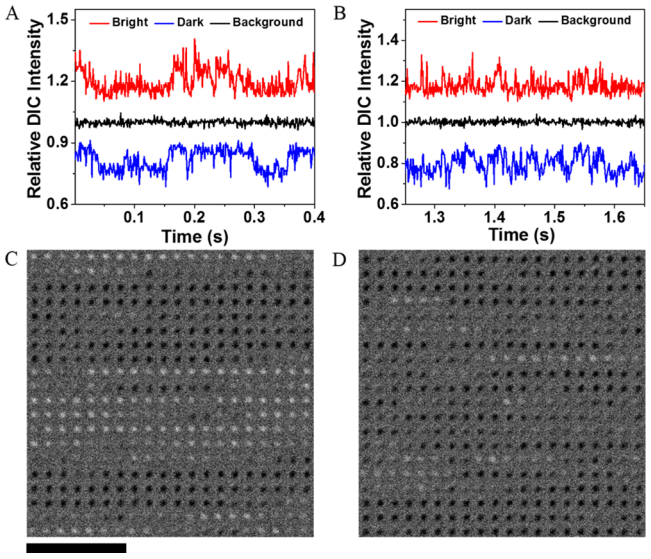

Figure 2. Relative DIC intensity traces of (A) slow rotation and (B) fast rotation, corresponding to the shaded gray and green areas in Figure S5 in the Supporting Information. Four hundred (400) consecutive recorded DIC images for (A) and (B) are stitched together (from left to right and from top to bottom) and shown as (C) and (D), respectively. Scale bar is 5 μm.

plasmonic bands at 339, 400, 506, and 563 nm. The rise of two higher energy bands at shorter wavelengths is believed to be due to the octupolar plasmonic modes, with the peaks at 506 and 575 nm corresponding to the transverse and longitudinal dipolar plasmonic modes.[25,27,28] At higher Ag/Au molar ratios, the rod shape was no longer maintained and a large fraction of irregular silver shells was observed (data not shown). Only the rod-shaped Au/AgNRs made with the Ag/Au molar ratio of 0.11 were used in the following synthesis and imaging experiments.

In order to improve the stability and reduce the intrinsic toxicity of silver, a dense silica layer was added as the last synthetic step. Figure 1 compares the normalized UV−vis extinction spectra of AuNRs, Au/AgNRs, and Au/Ag/SiO_2−NRs. In these measurements, the colloidal solutions were kept at the same concentration to minimize the dilution effect. Figure 1 (inset) shows a representative TEM image of the core−shell structure with average dimensions of ~46 nm × 64 nm. Due to the relatively low lattice mismatch (0.27%) of the two metals, the Ag shells grow almost perfectly upon the AuNRs through epitaxial deposition. We also found that the Ag shell thickness increases faster along the lateral direction than at the tips, which leads to the reduction of the aspect ratio of Au/AgNRs from the original AuNRs. In view of their relative extinction intensities, the longitudinal dipolar plasmonic mode increases by roughly a factor of 3 in Au/AgNRs compared to that of the original AuNRs. The baseline in the UV−vis extinction spectrum of the Au/Ag/SiO_2−NR solution is elevated because of scattering caused by silica, as reported previously.[33]

Following the synthesis, the Au/Ag/SiO_2−NRs were imaged under a DIC microscope equipped with a Hamamatsu ORCA-Flash 2.8 scientific CMOS camera, which allows imaging at millisecond or submillisecond temporal resolution. In addition to the enhanced LSPR response from the silver coating, the blue shift of the LSPR wavelength from 632 nm (AuNRs) to

DOI: 10.1021/acs.analchem.5b00604
Anal. Chem. 2015, 87, 4096−4099

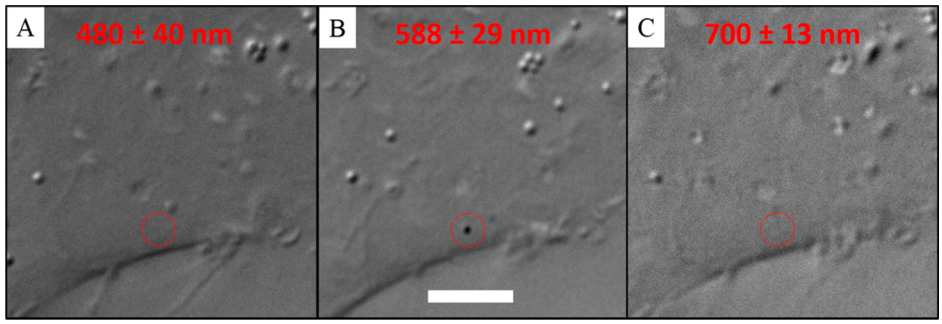

Figure 3. Differentiation of the Au/Ag/SiO_2−NRs (highlighted in the red circles) from other cellular features using three filters, (A) 480 ± 40 nm, (B) 588 ± 29 nm, and (C) 700 ± 13 nm. Scale bar is 4 μm. These images were taken sequentially. The nanorod and many cellular features changed their location and/or morphology during the imaging time.

563 nm provides another noticeable gain in the camera's quantum efficiency and therefore sensitivity.

In our previous studies, the DIC contrasts, defined as the difference between the brightest and the darkest intensities divided by the average local background intensity, of nanoparticles were shown to be wavelength dependent and the longitudinal LSPR was more sensitive to the environment than the transverse LSPR.[18,38] Herein, the DIC contrast of an immobilized, randomly oriented Au/Ag/SiO_2−NR is plotted as a function of excitation wavelength (Figure S3 in the Supporting Information). The highest DIC contrast for this particle was found when a 585 ± 29 nm filter was used for illumination, which corresponds to the longitudinal dipolar plasmonic band.

DIC images of two immobilized Au/Ag/SiO_2−NRs on glass slides were recorded at different exposure times and stitched together to make Movie S1 in the Supporting Information, which is played at 30 frames per second (fps). These two particles in the movie were nearly perpendicular to each other as their DIC images showed the totally bright and totally dark patterns. During these measurements, the light source was kept at the maximum output power (100 W), and the overall intensity decreased linearly as expected when shorter exposure time was used (Figure S4 in the Supporting Information). The relative bright and dark intensity measurement errors were increased from ∼1% at 50 ms to ∼5% at 0.5 ms for both nanorods (Table S1 in the Supporting Information). Because of the LSPR enhancement due to the silver coating, the core−shell hybrid nanorods were detectable at a temporal resolution as fast as 0.5 ms, which is approximately an order of magnitude faster than the previously reported fastest temporal resolution of 2−5 ms.[5,19]

A 360° rotation study of the Au/Ag/SiO_2−NRs was carried out by rotating the sample stage with 10° increments to position the nanorods in different orientations while exciting at the longitudinal LSPR wavelength of 563 nm. The orientation angle φ was defined as the angle between the long axis of the nanorod and the "dark" polarization direction of the DIC microscope (Figure S5A in the Supporting Information). The "bright" polarization direction is named after the fact that a completely bright DIC image is obtained when the nanorod's long axis aligns with this polarization direction (φ = 0), while the "dark" polarization direction corresponds to a completely dark DIC image. Figure S5B in the Supporting Information shows the complete rotation set of disproportionate bright and dark DIC image patterns. The DIC images change periodically as the nanorod's long axis rotates against the polarization directions. This is in good agreement with the polarization-dependent rotation behaviors of plasmonic nanoparticles that have been extensively investigated in gold nanorods and nanowires.[18,39] In view of the periodic changes, a correlation between the bright and dark intensity traces is observed: the bright and dark intensities increase and decrease in the same direction. This orientation/polarization dependence is the foundation for the use of Au/Ag/SiO_2−NRs as SPORT probes.

Dynamic tracking of the Au/Ag/SiO_2−NRs was first performed on synthetic lipid bilayers. The nanorods were introduced onto the synthetic lipid bilayers in a chamber and bound to the membrane through nonspecific interactions. Movies were recorded at a temporal resolution of 1 ms under 588 ± 29 nm illumination. Figure S6 in the Supporting Information shows the DIC intensity traces extracted from a representative 4 s (4000 frames) movie. The autocorrelation analysis of the DIC bright and dark traces[19] reveals that the nanorod's rotation speed fluctuates constantly. Representative examples of slow and fast rotation are given in Figure 2. The mean relaxation times of these two cases are 0.59 s (slow) and 0.024 s (fast).

To demonstrate the suitability of the new rotational probes for live-cell imaging, A549 human lung cancer cells were used as a model system, which provided a dynamic surface for rotational studies. Despite the much more complex cellular environments, the wavelength dependent properties of these SPORT probes are easily distinguished from other cellular features by using different band-pass filters. Three band-pass filters (480 ± 40 nm, 588 ± 29 nm, and 700 ± 13 nm) were used to identify the nanorods. As shown in Figure 3, the 588 ± 29 nm filter, which covers the longitudinal LSPR band, results in a high-contrast DIC image of Au/Ag/SiO_2−NRs that is distinct from the background. With either 480 ± 40 nm or 700 ± 13 nm band-pass filters, the Au/Ag/SiO_2−NRs disappear into the background due to the low contrast achieved at these wavelengths, which are far away from the LSPR bands.

In the live-cell imaging experiments, the Au/Ag/SiO_2−NRs were added into a chamber with A549 cells attached on the coverslip. Movies of the dynamic rotation of these nanorods were recorded at different exposure times of 1, 5, and 50 ms. The DIC intensity traces and the corresponding sets of consecutive DIC images were plotted in Figure S7 in the Supporting Information. The autocorrelation analysis of the DIC bright and dark traces gives mean relaxation times of 11 ms at the temporal resolution of 1 ms, 23 at 5 ms, and 115 at 50 ms. Higher temporal resolution helps to unveil fast rotational

DOI: 10.1021/acs.analchem.5b00604
Anal. Chem. 2015, 87, 4096−4099

dynamics, even though the overall intensity inevitably decreases as the single-frame exposure time decreases.

In summary, we have successfully synthesized Au/Ag/SiO_2−NRs with well-controlled size and shape for SPORT. These optically anisotropic hybrid plasmonic nanorods exhibit orientation/polarization and wavelength dependent behavior in DIC microscopy. With the enhancement of the longitudinal dipolar LSPR after silver coating, these nanorods provide sufficient sensitivity for detection at millisecond temporal resolution on both synthetic lipid bilayers and live cell membranes. Surface modification of the silica layer of the hybrid nanorods will enable versatile applications in SPORT.

■ ASSOCIATED CONTENT

Ⓢ Supporting Information

Experimental details, additional figures, and a movie as mentioned in the text. This material is available free of charge via the Internet at http://pubs.acs.org.

■ AUTHOR INFORMATION

Corresponding Authors

*E-mail: vela@iastate.edu.

*E-mail: nfang@iastate.edu.

Author Contributions

†K.C. and C.-C.L. contributed equally to this work.

Notes

The authors declare no competing financial interest.

■ ACKNOWLEDGMENTS

This research is supported by the U.S. Department of Energy, Office of Basic Energy Sciences, Division of Chemical Sciences, Geosciences, and Biosciences through the Ames Laboratory. The Ames Laboratory is operated for the U.S. Department of Energy by Iowa State University under Contract No. DE-AC02-07CH11358. The authors thank Michelle Thompson for assistance.

■ REFERENCES

(1) Saxton, M. J.; Jacobson, K. *Annu. Rev. Biophys. Biomol. Struct.* **1997**, *26*, 373−399.

(2) Fujiwara, T.; Ritchie, K.; Murakoshi, H.; Jacobson, K.; Kusumi, A. *J. Cell Biol.* **2002**, *157*, 1071−1081.

(3) Lakadamyali, M.; Rust, M. J.; Babcock, H. P.; Zhuang, X. *Proc. Natl. Acad. Sci. U.S.A.* **2003**, *100*, 9280−9285.

(4) Yezhelyev, M. V.; Qi, L.; O'Regan, R. M.; Nie, S.; Gao, X. *J. Am. Chem. Soc.* **2008**, *130*, 9006−9012.

(5) Gu, Y.; Sun, W.; Wang, G.; Jeftinija, K.; Jeftinija, S.; Fang, N. *Nat. Commun.* **2012**, *3*, 1030.

(6) Greeson, J. N.; Raphael, R. M. *J. Biomed. Opt.* **2007**, *12*, 021002−021009.

(7) Beausang, J. F.; Sun, Y.; Quinlan, M. E.; Forkey, J. N.; Goldman, Y. E. *Cold Spring Harbor Protoc.* **2012**, *2012*, 535−545.

(8) Chung, I.; Shimizu, K. T.; Bawendi, M. G. *Proc. Natl. Acad. Sci. U.S.A.* **2003**, *100*, 405−408.

(9) Toprak, E.; Enderlein, J.; Syed, S.; McKinney, S. A.; Petschek, R. G.; Ha, T.; Goldman, Y. E.; Selvin, P. R. *Proc. Natl. Acad. Sci. U.S.A.* **2006**, *103*, 6495−6499.

(10) Sönnichsen, C.; Alivisatos, A. P. *Nano Lett.* **2004**, *5*, 301−304.

(11) Chang, W.-S.; Ha, J. W.; Slaughter, L. S.; Link, S. *Proc. Natl. Acad. Sci. U.S.A.* **2010**, *107*, 2781−2786.

(12) Tcherniak, A.; Dominguez-Medina, S.; Chang, W.-S.; Swanglap, P.; Slaughter, L. S.; Landes, C. F.; Link, S. *J. Phys. Chem. C* **2011**, *115*, 15938−15949.

(13) Li, T.; Li, Q.; Xu, Y.; Chen, X. J.; Dai, Q. F.; Liu, H.; Lan, S.; Tie, S.; Wu, L. J. *ACS Nano* **2012**, *6*, 1268−1277.

(14) Zhang, B.; Lan, T.; Huang, X.; Dong, C.; Ren, J. *Anal. Chem.* **2013**, *85*, 9433−9438.

(15) Marchuk, K.; Ha, J. W.; Fang, N. *Nano Lett.* **2013**, *13*, 1245−1250.

(16) Stender, A. S.; Marchuk, K.; Liu, C.; Sander, S.; Meyer, M. W.; Smith, E. A.; Neupane, B.; Wang, G.; Li, J.; Cheng, J.-X.; Huang, B.; Fang, N. *Chem. Rev.* **2013**, *113*, 2469−2527.

(17) Ha, J. W.; Marchuk, K.; Fang, N. *Nano Lett.* **2012**, *12*, 4282−4288.

(18) Wang, G.; Sun, W.; Luo, Y.; Fang, N. *J. Am. Chem. Soc.* **2010**, *132*, 16417−16422.

(19) Gu, Y.; Sun, W.; Wang, G.; Fang, N. *J. Am. Chem. Soc.* **2011**, *133*, 5720−5723.

(20) Gu, Y.; Ha, J. W.; Augspurger, A. E.; Chen, K.; Zhu, S.; Fang, N. *Nanoscale* **2013**, *5*, 10753−10764.

(21) Nikoobakht, B.; El-Sayed, M. A. *Chem. Mater.* **2003**, *15*, 1957−1962.

(22) Gole, A.; Murphy, C. J. *Chem. Mater.* **2004**, *16*, 3633−3640.

(23) Jana, N. R.; Gearheart, L.; Murphy, C. J. *Chem. Commun.* **2001**, 617−618.

(24) Pietrobon, B.; McEachran, M.; Kitaev, V. *ACS Nano* **2008**, *3*, 21−26.

(25) Liu, M.; Guyot-Sionnest, P. *J. Phys. Chem. B* **2004**, *108*, 5882−5888.

(26) Xiang, Y.; Wu, X.; Liu, D.; Li, Z.; Chu, W.; Feng, L.; Zhang, K.; Zhou, W.; Xie, S. *Langmuir* **2008**, *24*, 3465−3470.

(27) Park, K.; Drummy, L. F.; Vaia, R. A. *J. Mater. Chem.* **2011**, *21*, 15608−15618.

(28) Jiang, R.; Chen, H.; Shao, L.; Li, Q.; Wang, J. *Adv. Mater.* **2012**, *24*, OP200−OP207.

(29) Hou, S.; Hu, X.; Wen, T.; Liu, W.; Wu, X. *Adv. Mater.* **2013**, *25*, 3857−3862.

(30) Zhu, J.; Zhang, F.; Li, J.-J.; Zhao, J.-W. *Gold Bull.* **2014**, *47*, 47−55.

(31) Damm, C.; Segets, D.; Yang, G.; Vieweg, B. F.; Spiecker, E.; Peukert, W. *Small* **2011**, *7*, 147−156.

(32) Cheng, X.; Zhang, W.; Ji, Y.; Meng, J.; Guo, H.; Liu, J.; Wu, X.; Xu, H. *RSC Adv.* **2013**, *3*, 2296−2305.

(33) Kobayashi, Y.; Katakami, H.; Mine, E.; Nagao, D.; Konno, M.; Liz-Marzán, L. M. *J. Colloid Interface Sci.* **2005**, *283*, 392−396.

(34) Sendroiu, I. E.; Warner, M. E.; Corn, R. M. *Langmuir* **2009**, *25*, 11282−11284.

(35) Mahanti, M.; Basak, D. *RSC Adv.* **2014**, *4*, 15466−15473.

(36) Aryal, S.; R, B. K. C.; Dharmaraj, N.; Bhattarai, N.; Kim, C. H.; Kim, H. Y. *Spectrochim. Acta, Part A* **2006**, *63*, 160−163.

(37) Khalavka, Y.; Becker, J.; Sonnichsen, C. *J. Am. Chem. Soc.* **2009**, *131*, 1871−1875.

(38) Ha, J. W.; Sun, W.; Stender, A. S.; Fang, N. *J. Phys. Chem. C* **2012**, *116*, 2766−2771.

(39) Ha, J. W.; Chen, K.; Fang, N. *Chem. Commun.* **2013**, *49*, 11038−11040.

DOI: 10.1021/acs.analchem.5b00604
Anal. Chem. 2015, 87, 4096−4099